Spectroscopic characterization of an ultrashort-pulse-laser-driven Ar cluster target incorporating both Boltzmann and particle-in-cell models

M. E. Sherrill, J. Abdallah, Jr., and G. Csanak
Theoretical Division, Los Alamos National Laboratory, Los Alamos, New Mexico 87545, USA

E. S. Dodd
Applied Physics Division, Los Alamos National Laboratory, Los Alamos, New Mexico 87545, USA

Y. Fukuda, Y. Akahane, M. Aoyama, N. Inoue, H. Ueda, and K. Yamakawa
Advanced Photon Research Center, Japan Energy Research Institute (JAERI), 8-1 Umemidai, Kizu-cho, Souraku-gun, Kyoto 619-0215, Japan

A. Ya. Faenov, A. I. Magunov, T. A. Pikuz, and I. Yu. Skobelev
Multicharged Ions Spectra Data Center of VNIIFTRI, Mendeleevo, Moscow Region 141570, Russia
(Received 16 June 2005; revised manuscript received 21 February 2006; published 19 June 2006)

A model that solves simultaneously both the electron and atomic kinetics was used to generate a synthetic He_α and satellite x-ray spectra to characterize a high intensity ultrashort laser driven Ar cluster target experiment. In particular, level populations were obtained from a detailed collisional-radiative model where collisional rates were computed from a time varying electron distribution function obtained from the solution of the zero-dimensional Boltzmann equation. In addition, a particle-in-cell simulation was used to model the laser interaction with the cluster target and provided the initial electron energy distribution function (EEDF) for the Boltzmann solver. This study suggests that a high density average, $\langle N_a \rangle_{high}$, of 3.2×10^{20} cm^{-3} was held by the system for a time, $\delta\tau$, of 5.7 ps, and during this time the plasma was in a highly nonequilibrium state in both the EEDF and the ion level populations.

DOI: 10.1103/PhysRevE.73.066404 PACS number(s): 52.50.Jm, 52.70.La, 52.65.Rr, 36.40.Vz

I. INTRODUCTION

Intense ultrashort laser irradiated rare-gas cluster targets are of considerable interest due to their extensive x-ray emission in the keV energy range and their production of highly energetic electrons and ions [1–4]. Such qualities have led applied scientists to consider these targets as debris-free x-ray sources for nanolithography and biological imaging as well as ion and neutron sources.

Spectroscopic modeling of intense ultrashort laser irradiated targets has predominately relied on steady state models with electron energy distribution functions (EEDF) composed of a low temperature Maxwellian containing the bulk of the free electrons with a high temperature component constituting a small fraction of the total population. Though this type of model has been successful at describing the effects of hot electrons on the x-ray spectra, it relies on the unrealistic assumption that the EEDF is in steady state [5].

In this work, a coupled electron kinetic and collisional-radiative model has been used to describe the time evolution of the EEDF, level populations, and x-ray spectra beginning immediately after the end of the main laser pulse and ending at an estimated time, $\delta\tau$, when the density of the expanding cluster is expected to fail to produce, to any spectroscopically significant amount, He- and Li-like transitions in the He_α spectrum. This period of time, for the purpose of this paper, will be referred to as the after glow phase (AGP). To model the interaction of the main laser pulse with the cluster, and to obtain a realistic EEDF at the beginning of the AGP, a particle-in-cell (PIC) code was used.

This EEDF adds an additional constraint on the coupled kinetic model and provides a more realistic view of the evolution of the cluster target during the AGP [6]. This model reveals a plasma, even at the end of the AGP, that is far from equilibrium in regard to the EEDF and far from steady state for the level populations. In addition, this model suggests an explanation for the insensitivity of the He_α spectrum above a critical laser intensity threshold observed in experiment.

II. EXPERIMENT

The Ar cluster experiments were performed with the JAERI (Kyoto, Japan) 100 TW Ti:sapphire laser system based on the technique of chirped pulse amplification, which was designed to generate 20 fs pulses at a 10 Hz repetition rate and is capable of producing a focused intensity up to 10^{20} W/cm^2 [7,8]. The laser pulses centered at 800 nm were generated at 82.7 MHz by a Ti:sapphire laser oscillator (10 fs). The pulses from the oscillator were stretched to 10 ns, and amplified by a regenerative amplifier and two stages of a multipass amplifier. In this study the amplified pulses were compressed to 30 fs by a vacuum pulse compressor yielding a maximum pulse energy of 360 mJ. In addition, after the regenerative amplifier, the pulse is passed through a double Pockels cells to reduce the prepulse. The final contrast ratio between the main pulse and the prepulse, which precedes it by 10 ns, is greater than $10^5:1$.

In a vacuum target chamber, the measured spot size was 11 μm at $1/e^2$, which was 1.1 times as large as that of the diffraction limit. Approximately 64% of the laser energy was

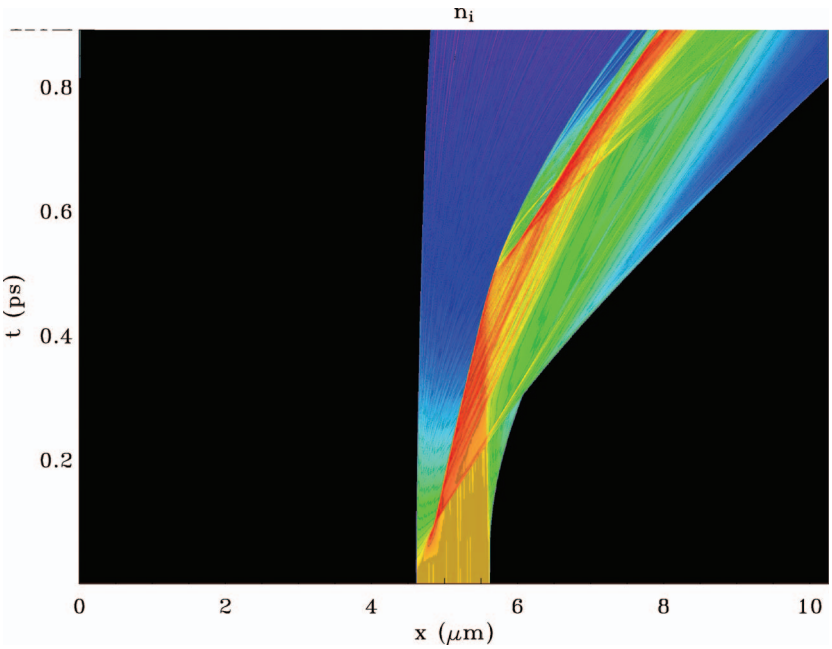

FIG. 1. (Color) Beginning at the end of the laser prepulse, the TRISTAN code simulates the evolution of the atom number density N_a during the main pulse phase and partial into the AGP. During the main pulse, the first 30 fs, the cluster appears motionless as it is radiated from the left-hand side. During the AGP, the ablation of material on the left-hand side pushes the cluster to the right-hand side of the figure. In addition, this thrust produces a high density region (yellow and red) that is seen to persist.

contained in the 11 μm Gaussian spot. These parameters give a focused laser peak intensity of 1.0×10^{19} W/cm^2 with a pulse duration of 30 fs and a pulse energy of 200 mJ.

Ar clusters were produced by expanding high-pressure (6 MPa) Ar gas into vacuum through a specially designed pulsed conical nozzle with input and output diameters of 0.5 and 2.0 mm, respectively, and a length of 75 mm. The parameters of this nozzle were calculated using a model developed at the Institute of Mathematical Modeling of the Russian Academy of Sciences [9,10]. The results of this model have been shown to be consistent with experimentally obtained data [5,11]. In particular, comparisons of Ar gas density spatial distribution—measured by interferometry, and the spatial distribution of cluster sizes—measured by light scattering diagnostics—have demonstrated the predictive capability of this code.

Simulations of the nozzle employed in this experiment and x-ray emission analysis of similar experiments suggest the production of a dense cluster medium with clusters approximately 1 μm in size [6,12–14]. Since the rate of cluster decay is primarily determined by the number of atoms in the cluster, the use of large clusters in conjunction with the prepulse reduction techniques insured the direct interaction between the high-density cluster and the main fs pulse. The laser was then focused about 1.5 mm below the nozzle.

The spatially resolved x-ray spectra were measured using focusing spectrometers with spatial resolution [15]. The spherically bent crystal was placed at a distance of 381.2 mm from the plasma source and was centered at $\lambda=4.05$ Å, which corresponds to a Bragg angle of 35.7° for fourth order reflection of the crystal. This instrument recorded He-like α spectra of Ar including the associated satellite lines [14].

III. THEORETICAL METHOD

A coupled nonrelativistic electron kinetic and collisional-radiative (CR) model was used to characterize this experi-

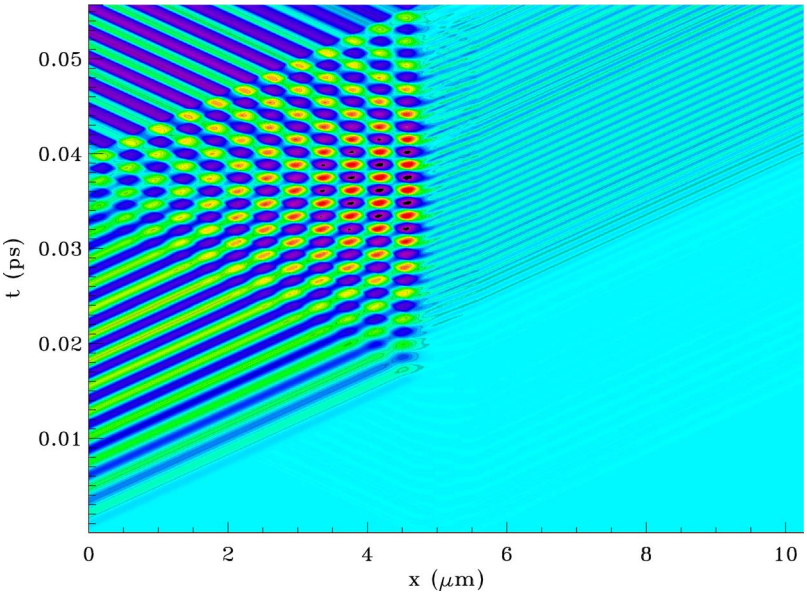

FIG. 2. (Color online) The electric field of the 30 fs main pulse was computed by a 1D PIC simulation. This figure displays the large degree of reflected intensity as the laser propagates from the left-hand side and interacts with the cluster located between 4.5 and 5.5 μm. Only a thin shell of the left-hand side of the cluster is directly exposed to the full laser intensity while a significantly reduced electric field ($E=1\times10^{10}$ V/cm^2) has transmitted through the cluster—as seen in the right-hand side of the figure. The cluster remained stationary during this short time duration.

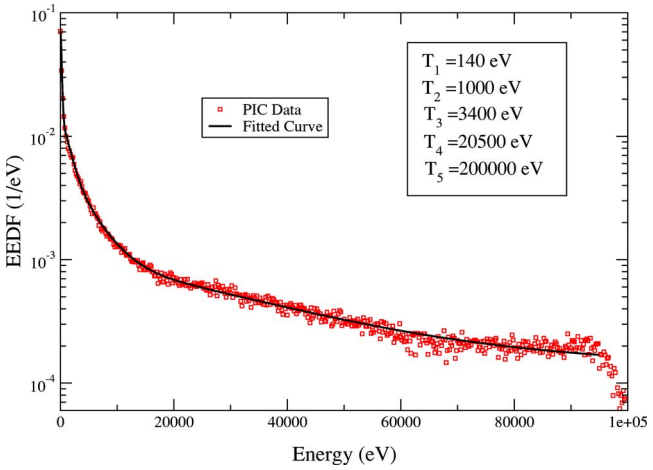

FIG. 3. (Color online) PIC produced, non-normalized EEDF at the end of the main laser pulse. Included are the five Maxwellian temperatures used to produce the best fit curve through the data to provide a smooth input EEDF for the Boltzmann solver.

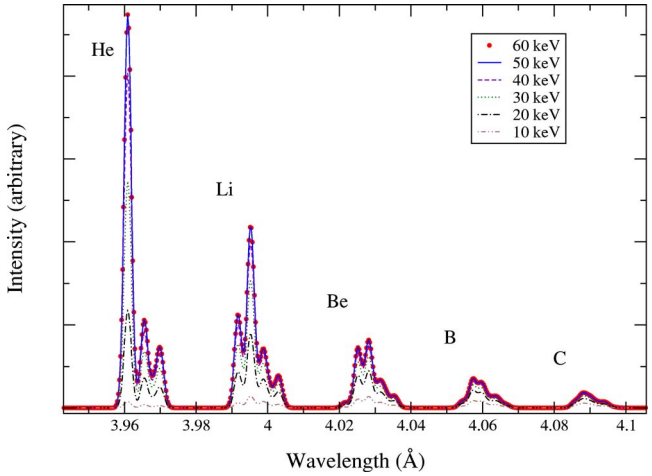

FIG. 4. (Color online) Effects on the time integrated He_α and satellite spectra including increasingly larger amounts of the EEDF in the spectroscopic calculation. A configuration average model was used in this study.

ment [16]. The atomic structure data produced for this model constituted over 3000 fine-structure levels spanning the Ne-like to He-like ionization stages. Atomic configurations up to principal quantum number $n=3$, and all x-ray transitions from $n=2$ to $n=1$ within the $n=3$ manifold were computed.

With time discretized, the evolution of the system was computed by first propagating the electron kinetics from time t to $t+\delta t$ (with a frozen set of level populations computed from the CR model for time t) to obtain EEDF and then propagating the CR model from time t to $t+\delta t$ (with the EEDF computed for time $t+\delta t$) to obtain the level populations.

Our electron kinetic model, following Bretagne *et al.* [17], solves the *zero-dimensional*, i.e., spatially independent, Boltzmann equation:

$$\frac{\partial f(E,t)}{\partial t} = \left(\frac{\partial f(E,t)}{\partial t}\right)_{coll}. \tag{1}$$

Included in the collision term are both elastic (electron-electron collisions) and inelastic (electron impact excitation, deexcitation and ionization) contributions:

$$\left(\frac{\partial f(E,t)}{\partial t}\right)_{coll} = \left(\frac{\partial f}{\partial t}\right)_{el(e\text{-}e)} + \left(\frac{\partial f}{\partial t}\right)_{in}. \tag{2}$$

To numerically solve the Boltzmann equation, the EEDF is approximated as a series of constant values within discrete energy bins

$$f(E,t) = f(E_u,t) \quad \text{for } E_u - \frac{w_u}{2} \leqslant E \leqslant E_u + \frac{w_u}{2},$$
$$\text{where } u = 1, \ldots, N_b. \tag{3}$$

In Eq. (3), f is the EEDF (the number of free electrons per unit energy interval per unit volume), E_u is the midpoint of the uth bin, w_u is the width of the uth bin, and N_b is the total number of bins. From this bin representation, the Boltzmann equation may be written as a coupled set of first order differential equations. Equation (4) describes the change of electron population in energy bin u by collisional processes contained in matrix elements $M_{u,v}(t)$ that involve the electrons from all the other energy bins:

$$\frac{d}{dt}f(E_u,t) = \sum_{v=1}^{N} M_{u,v}(t) f(E_v,t). \tag{4}$$

The PIC code used to model the main pulse phase of the laser-cluster interaction was a one-dimensional (1D) version of the TRISTAN code [18,19]. [1] This code propagated, in a fully relativistic manner, 163,840 plasma particles in the self-consistent fields produced by both the laser and the plasma resulting from a single irradiated cluster. This version of TRISTAN contains neither field ionization nor collision physics. Therefore, we have assumed a constant average ion charge $\langle Z\rangle = 8$ that corresponds to the assumed prepulse of the prepared Ne-like Ar plasma. For the atomic number densities considered, the corresponding ratio of N_e/N_{cr} varied from 0.81 to 25.8. Furthermore, due to an observed insensitivity to the shape of the EEDF for plasmas within this density range,[2] the EEDF was computed for an average density case ($N_a = 6.0\times 10^{20}$ cm^{-3}) and normalized to the free electron population of each case.

[1] Within the uncertainties imposed by our assumptions of the initial conditions of the cluster plasma, the 1D TRISTAN code should accurately model the coupling between the 30 fs main laser pulse and the relatively stationary prepulse prepared cluster plasma. The 1D nature of this code, however, precludes it from accurately predicting the long term expansion of the cluster that is inherently three dimensional.

[2] Though the mechanism that couples the laser energy to the plasma differs for below critical and above critical targets, the values for the N_e/N_{cr} ratio chosen in this work did not alter, to any significant degree, the *shape* of the EEDF.

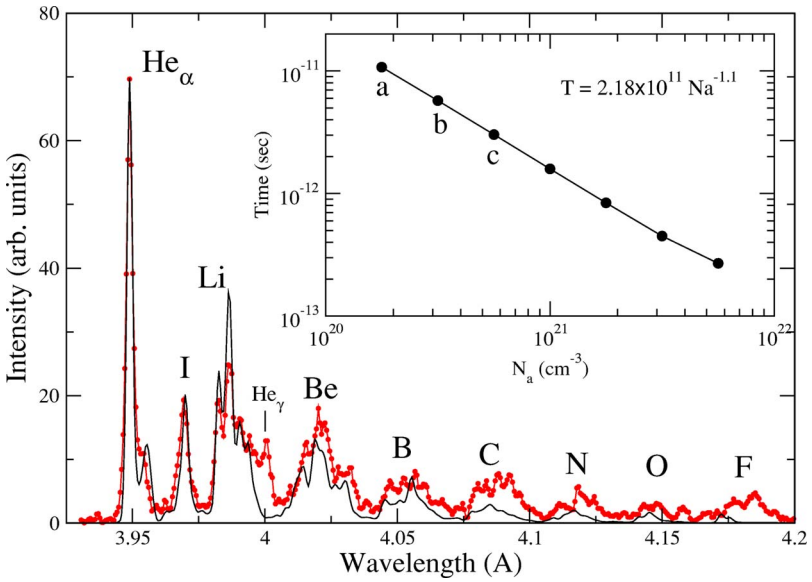

FIG. 5. (Color online) Synthetic (black line) and experimental (red points) time integrated He$_\alpha$ and satellite spectra for Case (b): $N_a=3.162\times10^{20}$ cm^{-3}, $\delta\tau=5.7$ ps. Inset contains least squares best fit for different N_a and their corresponding AGP termination times. In particular, (a) $N_a=1.8\times10^{20}$ cm^{-3}; (b) $N_a=3.2\times10^{20}$ cm^{-3}; (c) $N_a=5.6\times10^{20}$ cm^{-3}.

IV. DISCUSSION AND RESULTS

Current modeling capabilities are unable to perform an end-to-end simulation of the above experiment. However, the x-ray spectra recorded during this experiment provides a signature for the *high* density state of the plasma as it evolves during the AGP. The modeling set forth here is designed to obtain *this* mean atom-number density, $\langle N_a\rangle_{high}$ (that we assume begins at the end of the prepulse and continues through the end of the AGP) and the time duration of the AGP, $\delta\tau$. In short, an iterative search procedure has been created to compare time integrated synthetic spectra to the experimental spectrum by varying the $\langle N_a\rangle_{high}$ and $\delta\tau$. Once an acceptable comparison has been obtained the detailed behavior of the high density component of the plasma as it evolves through the AGP can be extracted.

For the purpose of this model, the time history of the irradiated cluster has been considered to evolve in three phases: prepulse phase, main pulse phase and the AGP. Beginning with a cold target, a 10 ns prepulse transforms the cluster target into a plasma with a moderately dense core:[3] we have assumed the system was left in a Ne-like Ar plasma state with a free-electron temperature of ~140 eV.[4] Strong emission observed in the experimental spectra from doubly excited states in the Li-like feature (q, r, and a-d) suggest that the high energy electrons produced by the main pulse and *not* the low temperature electrons produced by the prepulse are responsible for ionizing the plasma through the L-shell series of ions. In addition, the strength of the features reveals the existence of a sustained high electron impact excitation and ionization rates that testify to the existence of a persistent dense plasma core remaining after the prepulse and on through the AGP. The existence of this persistent dense plasma region is also supported by the 1D PIC simulations, Fig. 1.

Throughout the 30 fs main pulse, the plasma remains in a Ne-like Ar state. PIC simulation results, Fig. 2, in conjunction with a tunneling ionization model [20,21] predict that the *bulk* plasma electric field ($E=1\times10^{10}$ V/cm^2) is too low to field ionize the L-shell ions; in addition, the 30 fs duration of the main pulse is too short for collisional processes to significantly alter the ionization balance of the target. Although the ionization balance will remain unchanged during this phase, the EEDF has been shown, through PIC simulations, to become highly nonthermal as in Fig. 3.

Beginning at the end of the laser pulse is the AGP. All the spectral modeling performed in this work pertains to this phase. To initialize the collisional-radiative model the ion populations are assumed to be in the ground state of Ne-like Ar, while the EEDF obtained from PIC simulations is used to initialize the Boltzmann solver.

Figure 3 is the non-normalized EEDF computed by the PIC code just after the end of the laser pulse. Due to the extensive computer memory requirements to run the Boltzmann solver, the entire EEDF produced by the PIC code could not be used. Therefore a minimum extent of the EEDF had to be determined that produced a convergent time integrated He$_\alpha$ spectrum; consequently, this study revealed the role of the high energy tail of the EEDF to the spectra. In Fig. 4, the spectrum was shown to converge only when the maximum energy of the EEDF included in the spectral calculation was above 50 keV; this corresponds to an energy approximately 50 times the Li-like Ar ionization potential ($I_p=918$ eV). In addition, the spectra appear to differ only by

[3]We have assumed that the single cluster plasma after the prepulse retains its 1 μm size. Though this may seem unphysical, the critical quality for this analysis is the atom number density. In addition, 1D PIC simulations of the interaction of the main pulse with the prepulse generated plasma are relatively insensitive to reasonable variations in the size of the plasma.

[4]The analysis employed here is insensitive to this initial temperature due to the dominant influence that the main pulse has on the EEDF.

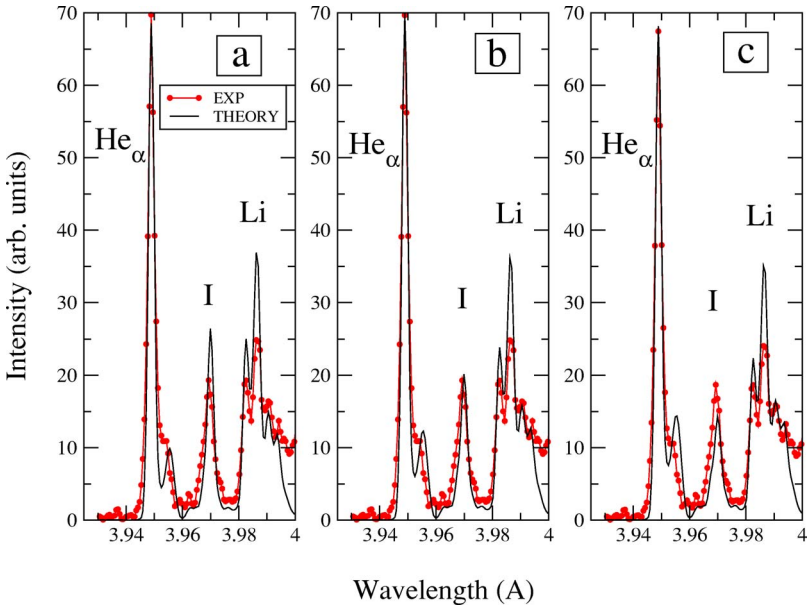

FIG. 6. (Color online) The sensitivity of the intensity of the intercombination line (**I**) relative to the He$_\alpha$ line. The cases shown here correspond to those found in the inset of Fig. 5: (a) $N_a=1.8\times10^{20}$ cm^{-3}; (b) $N_a=3.2\times10^{20}$ cm^{-3}; (c) $N_a=5.6\times10^{20}$ cm^{-3}.

a proportionality constant, in particular for E_{max} above 30 keV. The insensitivity of the shape of the spectrum has been observed experimentally in studies when the total pulse energy has been varied [13]. The consistency of these two results suggests that an increase in laser energy simply promotes free electrons into the very high energy tail of the EEDF. Though this increases the overall intensity of the spectrum, it does not promote, to any significant degree, preferential ionization and excitation that may have led to relative changes in the spectral features.

As the irradiated cluster expands during the AGP phase, the time-integrated spectrum is expected to contain the cumulative contributions of radiation produced from several densities. The constant atomic number density (N_a) approximation imposed by our model prevents an accurate reproduction of the entire spectral range of the He$_\alpha$ spectrum as seen in Fig. 5.[5] Therefore we have concentrated our attention in determining a suitable maximum atomic density necessary to reproduce the high energy portion of the He$_\alpha$ spectrum.

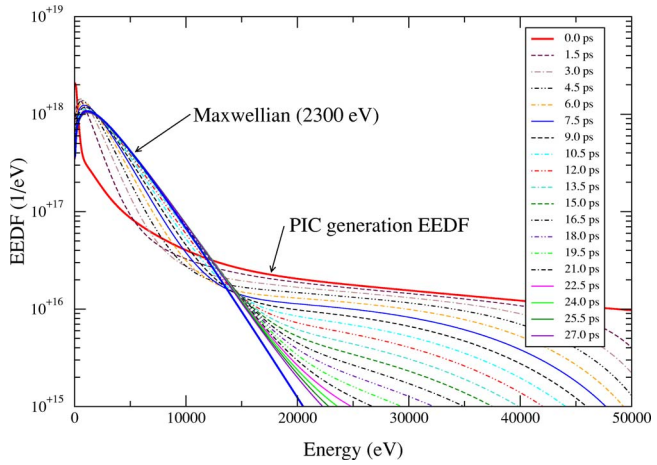

FIG. 7. (Color online) The time history of the EEDF, for times after the end of the laser pulse, computed for $N_a=3.162\times10^{20}$ cm^{-3}.

The inset in Fig. 5 displays the best least squares comparisons between the experimental spectrum and synthetic spectra for various constant atomic number densities and their corresponding AGP termination times. In this general comparison, the variation in the fitness of these optimal results was too small to conclusively select one overall best fit. This illustrates the ambiguity in using time integrated spectra to characterize these types of experiments.

However, the density sensitivity between the He$_\alpha$ resonance line and the intercombination line (**I**) in Fig. 6 suggests that the spectra produced with $N_a=3.162\times10^{20}$ cm^{-3} more closely resembles these high energy spectral features (the total spectrum is shown in Fig. 5).

Figure 7 describes the time history of the EEDF, after the end of the laser pulse, as computed by the Boltzmann solver for $N_a=3.162\times10^{20}$ cm^{-3}. During the evolution of the EEDF, the high energy tail characteristic of the PIC generated EEDF is reduced, while the population in the lower energy bins is increased. The generation of low energy electrons early in time is predominantly due to ejected and scattered electrons produced by electron impact ionization. Interestingly, the EEDF is far from equilibrium at the end of the AGP ($\delta\tau\sim5.7$ ps as predicted in Fig. 5). Furthermore, pseudo-thermalization of the free electrons occurs much later (after $T=27.0$ ps) if we allow the predicted constant density to continue.[6] To illustrate the extent that the $T=27.0$ ps EEDF result has obtained a thermal equilibrium solution,

[5]As reported in a similar experiment by Dorchies *et al.* [22], no emission is observed from the "cold" $K\alpha$ line indicating neutral atoms no longer exist during the AGP.

[6]Clearly this prediction is an upper limit to the thermalization time. The natural drop in the density due to the cluster expansion would be expected to further impede thermalization due to the subsequent fall in the collisional rates.

Fig. 7 contains a 2300 eV Maxwellian that has been predicted from two times the maximum of the 27.0 ps EEDF. In addition, to the non-Maxwellian EEDF at the end of the predicted AGP, ion level populations are far from equilibrium and continue to evolve long after the AGP.

V. CONCLUSIONS

In summary, the high density contribution of the AGP phase of an ultrashort laser driven Ar cluster experiment was characterized through spectral modeling and comparisons with a time-integrated He_α spectrum. Our spectral model incorporates both time-dependent atomic kinetics and electron kinetics to model this highly nonequilibrium plasma. In addition, PIC modeling was performed to model the 30 fs interaction between the main laser pulse and the cluster target. The results from the PIC simulation were then used to initialize the atomic-electronic kinetic model. We have obtained from our modeling an estimate of $\langle N_a \rangle_{high} = 3.162 \times 10^{20}$ cm^{-3} for the high density contribution to the AGP and acquired evidence that the plasma responsible for this experimental spectrum was far from equilibrium in both EEDF and ion level populations.

In addition, the full time-dependent spectral model revealed the interesting quality that the high energy electrons, above a critical threshold value, do not affect the shape of the time-integrated He_α spectrum. This consistent behavior of the shape of the He_α spectrum has been observed experimentally with increased laser pulse energy. This suggests that increasing the laser pulse energy predominantly drives the generation of high energy electrons, and these electrons do not preferentially drive ionization in the plasma.

ACKNOWLEDGMENTS

This work was supported under the auspices of the U.S. Department of Energy at Los Alamos National Laboratory under Contract No. W-7405-ENG-36.

[1] T. Ditmire, T. Donnelly, A. M. Rubenchik, R. W. Falcone, and M. D. Perry, Phys. Rev. A **53**, 3379 (1996).
[2] P. Gibbon, Plasma Phys. Controlled Fusion **38**, 769 (1996).
[3] T. Ditmire, J. Zweiback, V. P. Yanovsky, T. E. Cowan, G. Hays, and K. B. Wharton, Nature (London) **398**, 489 (1999).
[4] E. Parra, I. Alexeev, J. Fan, K. Kim, S. J. McNaught, and H. M. Milchberg, Phys. Rev. E **62**, R5931 (2000).
[5] G. C. Junkel-Vives, J. Abdallah, Jr., T. Auguste, P. D'Oliveira, S, Hulin, P. Monot, S. Dobosz, A. Ya Faenov, A. I. Magunov, T. A. Pikuz, I. Yu. Skobelev, A. S. Boldarev, and V. A. Gasilov, Phys. Rev. E **65**, 036410 (2002).
[6] J. Abdallah, Jr., G. Csanak, Y. Fukuda, Y. Akahane, M. Aoyama, N. Inoue, H. Ueda, K. Yamakawa, A. Ya. Faenov, A. I. Magunov, T. A. Pikuz, and I. Yu. Skobelev, Phys. Rev. A **68**, 063201 (2003).
[7] K. Yamakawa, M. Aoyama, S. Matsuoka, T. Kase, Y. Akahane, and H. Takuma, Opt. Lett. **23**, 1468 (1998).
[8] Y. Akahane, Ma. Jinlong, Y. Fukuda, M. Aoyama, H. Kiriyama, JV Sheldakova, AV Kudryashov, and K. Yamakawa, Rev. Sci. Instrum. **77**, 023102 (2006).
[9] A. S. Boldarev, V. A. Gasilov, and A. Ya. Faenov, JETP Lett. **73**, 514 (2001).
[10] A. S. Boldarev, V. A. Gasilov, and A. Ya. Faenov, Tech. Phys. **49**, 388 (2004).
[11] F. Dorchies, F. Blasco, T. Caillaud, J. Stevefelt, C. Stenz, A. S. Boldarev, and V. A. Gasilov, Phys. Rev. A **68**, 023201 (2003).
[12] Y. Fukuda, K. Yamakawa, Y. Akahane, M. Aoyama, N. Inoue, H. Ueda, J. Abdallah, Jr., G. Csanak, A. Ya. Faenov, A. I. Magunov, T. A. Pikuz, I. Yu. Skobelev, A. S. Boldarev, and V. A. Gasilov, JETP Lett. **78**, 115 (2003).
[13] Y. Fukuda, Y. Akahane, M. Aoyama, N. Inoue, H. Ueda,Y. Kishimoto, K. Yamakawa, A. Ya. Faenov, A. I. Magunov, T. A. Pikuz, I. Yu. Skobelev, J. Abdallah, Jr., G. Csanak, A. S. Boldarev, and V. A. Gasilov, Proc. SPIE **5196**, 234 (2004).
[14] Y. Fukuda, Y. Akahane, M. Aoyama, N. Inoue, H. Ueda, Y. Kishimoto, K. Yamakawa, A. Ya. Faenov, A. I. Magunov, T. A. Pikuz, I. Yu. Skobelev, J. Abdallah, Jr., G. Csanak, A. S. Boldarev, and V. A. Gasilov, Laser Part. Beams **22**, 215 (2004).
[15] A. Y. Faenov, S. A. Pikuz, A. I. Erko, B. A. Bryunetkin, V. M. Dyakin, G. V. Ivanenkov, A. R. Mingaleev, T. A. Pikuz, V. M. Romanova, and T. A. Shelkovenko, Phys. Scr. **50**, 33 (1994).
[16] M. E. Sherrill, J. Abdallah, Jr., G. Csanak, D. P. Kilcrease, E. S. Dodd, Y. Fukuda, Y. Akahane, M. Aoyama, N. Inoue, H. Ueda, K. Yamakawa, A. Ya. Faenov, A. I. Magunov, T. A. Pikuz, and I. Yu. Skobelev, J. Quant. Spectrosc. Radiat. Transf. **99**, 584 (2006).
[17] J. Bretagne, G. Delouya, J. Godart, and V. Puech, J. Phys. D **14**, 1225 (1981).
[18] E. S. Dodd, J. K. Kim, and D. Umstadter, Phys. Rev. E **70**, 056410 (2004).
[19] J. Villasenor and O. Buneman, Comput. Phys. Commun. **69**, 306 (1992).
[20] M. V. Ammosov, N. B. Delone, and V. P. Krainov, Sov. Phys. JETP **64**, 1191 (1985).
[21] B. M. Penetrante and J. N. Bardsley, Phys. Rev. A **43**, 3100 (1991).
[22] F. Dorchies, T. Caillaud, F. Blasco, C. Bonte, H. Jouin, S. Michaeu, B. Pons, and J. Stevefelt, Phys. Rev. E **71**, 066410 (2005).